International Journal of Pharmaceutics 586 (2020) 119569

Contents lists available at ScienceDirect

International Journal of Pharmaceutics

journal homepage: www.elsevier.com/locate/ijpharm

Nanostructured lipid carriers as oral delivery systems for improving oral bioavailability of nintedanib by promoting intestinal absorption

Yunjing Zhu[a,1], Xue Liang[a,1], Cong Lu[a], Yihan Kong[a], Xing Tang[a], Yu Zhang[a], Tian Yin[b], Jingxin Gou[a], Yanjiao Wang[a], Haibing He[a,*]

[a] Department of Pharmaceutics, College of Pharmacy, Shenyang Pharmaceutical University, Shenyang 110016, China
[b] School of Functional Food and Wine, Shenyang Pharmaceutical University, Shenyang 110016, China

ARTICLE INFO

Keywords:
Nintedanib
Nanostructured lipid carriers
Bioavailability
Oral

ABSTRACT

The aim of this study was to fabricate nanostructured lipid carriers, NLCs, of nintedanib (BIBF) to improve its oral bioavailability. Two types of NLCs loaded with BIBF (BIBF-NLCs-1 and BIBF-NLCs-2) were prepared by the melt-emulsification technique. BIBF-NLCs-1 and BIBF-NLCs-2 showed nanoscale particle sizes of 142.70 ± 0.85 nm and 7.99 ± 0.06 nm, and both were positive zeta potential. Study on Caco-2 cells showed that BIBF-NLCs-1 exhibited distinct advantages at the cytological level. The oral bioavailability of BIBF-NLCs-1 and BIBF-NLCs-2 was extremely improved 3.13-fold and 2.39-fold respectively compared with BIBF solution (BIBF-Sol). And *in vivo* anti-tumor efficiency study in mice bearing LLC lung tumor indicated that BIBF-NLCs-1 and BIBF-NLCs-2 had excellent tumor inhibition. Besides, the two NLCs did not increase the risk of liver damage and can even reduce the incidence of gastrointestinal irritation of BIBF to some extent. In summary, NLCs are a potential oral delivery system to improve the bioavailability of BIBF by promoting intestinal absorption.

1. Introduction

Nintedanib (BIBF 1120, abbreviated as BIBF) is a small molecule oral triple tyrosinase inhibitor, classified as a BCS II drug (Roth et al., 2015). It is a substrate for P-glycoprotein (P-gp) and has a hepatic first-pass effect (Vaidya et al., 2019), which suggests a possible efflux of BIBF during intestinal absorption which further contributes to its poor bioavailability. BIBF can potently block three proangiogenic pathways, achieved by targeting three tyrosinase receptors (Reck, 2015), which have been reported to play an important role in the pathogenesis of idiopathic pulmonary fibrosis (IPF) (Dimitroulis, 2014). Based on the satisfactory *in vitro* and *in vivo* anti-tumor, anti-angiogenic and anti-fibrotic effects, BIBF was approved by the US Food and Drug Administration (FDA) for the treatment of IPF in 2014. At the same time, BIBF has also been approved by the European Medicines Agency (EMA) for the treatment of non-small cell lung cancer (NSCLC) in combination with docetaxel (Reck et al., 2014). The current clinical application of BIBF is the soft capsule (Fukihara and Kondoh, 2016), Ofev®, which is developed, produced and marketed by the German Boehringer Ingelheim Company. According to their study, the bioavailability of a single-dose 100 mg BIBF soft capsule in healthy volunteers was approximately 4.69% (Vaidya et al., 2019), which is very poor. Hence, research to improve its oral bioavailability is critical.

Improving dissolution is a common and effective means to solve the poor oral bioavailability of BCS II drugs. However, as described in this study, the solid dispersion (SD) strategy was used in an attempt to improve the solubility of BIBF, however it did not increase oral bioavailability. This verified that simply increasing the rate and extent of dissolution could not effectively improve the bioavailability of BIBF, and thus other factors that lead to poor bioavailability of BIBF should be taken into account, such as intestinal absorption problems caused by P-gp efflux. Clinical reports have shown that the addition of P-gp inhibitors can effectively improve the bioavailability of BIBF (Vaidya et al., 2019).

Nanomedicine can be applied in drug delivery systems to promote drug dissolution, improve absorption, enhance targeting and more (Mishra et al., 2018a). Micelles, liposomes, solid lipid nanoparticles (SLNs) and nanoparticles (NPs) of biodegradable polymers are common forms of nanomedicine applications (Feng et al., 2011). Among them, SLNs were developed as a substitute for colloidal systems in the 1990s (Beloqui et al., 2016b). They have excellent tolerance due to the use of biodegradable lipids, and also have the advantages of being easily scale-

* Corresponding author at: Shenyang Pharmaceutical University, No.103, Wenhua Road, Shenyang 110016, China.
E-mail address: hhb_emily@126.com (H. He).
[1] Both authors contribute equally to this work.

https://doi.org/10.1016/j.ijpharm.2020.119569
Received 19 February 2020; Received in revised form 22 May 2020; Accepted 19 June 2020
Available online 24 June 2020
0378-5173/

up production, increasing drug stability (Mishra et al., 2018b). However, the relatively weak drug-loading capacity of SLNs, and drug leakage during storage, have limited their wider application (Muller et al., 2002; Pardeike et al., 2009). Thus, nanostructured lipid carriers (NLCs) were further developed. Based on the advantages of SLNs, NLCs have further improved drug-loading capacity and prevention of drug leakage (Iqbal et al., 2012). NLCs have liquid lipids incorporated in the original solid lipids. The introduction of liquid lipids destroys the perfect crystal form of SLNs, forming a less ordered or imperfect lattice, which facilitates the loading of the drug and thus improving the drawbacks of SLNs (Hu et al., 2006; Pastor et al., 2019).

It is extremely complex for the mechanism of the P-gp inhibition by the polymers, because they could inhibit the p-gp by reducing P-gp expression, inhibiting or stimulating the ATP enzyme of P-gp, and changing the fluidity of the cellular membrane. Ran Mo, *et al*, studied the mechanism of N-octyl-O-sulfate chitosan (NOSC) on P-gp inhibition and the results showed that by interfering the P-gp ATPase by NOSC rather than reducing the P-gp expression could improve the bioavailability of PTX (Mo et al., 2011).

In the past few years, various studies have demonstrated that NLCs are suitable for oral delivery of poorly water soluble P-gp substrates. Saquinavir(SQV) is a BCS class IV drug and P-gp substrate, a SQV loaded NLC of size 247 nm and 1.5% (w/v) surfactant content was incubated with the P-gp inhibitor verapamil for 2 h, however, it showed no difference in the permeability rates regardless of the presence or absence of verapamil. The result demonstrated that NLC formulation could circumvent the P-gp efflux, and use both caveolae- and clathrin-mediated transcytosis (Beloqui et al., 2017, 2013). Therefore, in the present work, in order to reduce P-gp efflux and improve intestinal absorption, BIBF-loaded NLCs (BIBF-NLCs) were prepared as drug delivery vehicles for improving the bioavailability and the anti-tumor effect of BIBF *in vivo*. Two different particle size NLCs were prepared separately with biocompatible lipids. The intestinal uptake of the two NLCs was studied and compared in terms of cell uptake and transmembrane transport. In addition, the oral bioavailability of BIBF-NLCs in rats was quantified and the anticancer effect was evaluated in a subcutaneous Lewis lung cancer mouse model. At present, there have been studies that successfully improved the bioactivity or therapeutic index of BIBF at the cellular level (Kallus et al., 2018; Vaidya et al., 2019). However, to the best of our knowledge, there are few studies on improving the oral bioavailability of BIBF by promoting intestinal absorption, and therefore this is an important and promising area.

2. Methods

2.1. Materials

Nintedanib ethanesulfonate (EHS) salt (> 99%) was kindly provided by Jiangsu Aosaikang Pharmaceutical Co., Ltd. (China). Lauroyl Macorgolglycerides and labrasol® were kindly provided by Gattefosse (Lyon, France). Tricaprylin was purchased from Sigma-Aldrich (Shanghai, China). Tween 80 and Poloxamer 407 were purchased from BASF (Ludwigshafen, Germany). Coumarin-6 was purchased from J$K Scientific Co., Ltd. (China). 4′, 6-diamidino-2-phenylindole (DAPI) was purchased from Dalian Meilun Biotechnology Co., Ltd. (Dalian, China).

All other chemicals and reagents were of analytical or chromatographic grade.

2.2. Cell line and animals

Caco-2 cell line and Lewis lung carcinoma (LLC) cell line were obtained from the Cell Bank of Chinese Academy of Sciences (Shanghai, China). Caco-2 and LLC cells were both maintained in high glucose DMEM medium, supplemented with 10% FBS in a humidified atmosphere containing 5% CO_2 at 37 ℃.

Sprague-Dawley rats (male, body weight: 200 g ± 20 g) and C57BL/6 mice (male, body weight: 18 g ± 2 g) were provided by Liaoning Changsheng Biotech Co., Ltd. (Benxi, China). All animal experiments were approved by the Animal Ethics Committee of Shenyang Pharmaceutical University (Ethical No. : SYPU-IACUC-C2019-10–28-202 (for part 1.8: *In vivo* pharmacokinetic study); SYPU-IACUC-S2019-09.23–102 (for part 1.9: *In vivo* antitumor effect and part 1.10: Gastrointestinal irritancy and liver damage)).

2.3. Preparation of two different BIBF NLCs and BIBF-Sol

The first type of NLCs loaded with BIBF (BIBF-NLCs-1) was prepared by the melt-emulsification technique as previously reported (Yuan et al., 2007) with some changes. Briefly, 1000 mg solid lipid (Glyceryl monooleate), 500 mg liquid lipid (Tricaprylin) and 528 mg emulsifier (Tween 80) were melted at 70 ˚C in a water bath and stirred for 5 min at 3000 rpm until homogeneous. Then, 50 mg BIBF was added to the mixture and stirred for a further 30 min. Subsequently, the aqueous phase was prepared with 132 mg cosurfactant (Poloxamer 407) completely dissolved in 8 mL ultrapure water, and then heated to the same temperature. The aqueous phase was slowly added dropwise into the hot lipid, and the mixture was emulsified at 3000 rpm for 5 min. The warm primary emulsion was further sonicated by a Lab ultrasonic cell pulverizer (SCIENTZ-IID, Scientz Biotechnology Co., Ltd., China) for 13 min (work 2 s and stand 2.5 s) at 285 W to form the miniemulsion. Finally, BIBF-NLCs-1 was obtained by cooling the samples in an ice water bath to quickly crystallize the lipid.

The second NLCs loaded with BIBF (BIBF-NLCs-2) was also prepared by the melt-emulsification technique, but with the ultrasound step omitted. Lauroyl Macorgolglycerides was used as the solid lipid and labrasol® as the liquid lipid. Tween 80 was employed instead of Poloxamer 407, and the preparation temperature was adjusted to 80 ˚C. The remaining steps were same as the preparation of BIBF-NLCs-1.

The corresponding blank BIBF-NLCs (abbreviated as Blank-1 and Blank-2, respectively) were prepared by the same method without addition of BIBF.

To compare BIBF-NLCs with BIBF-Sol, an BIBF-Sol was prepared. Briefly, the aqueous phase was prepared with 132 mg Tween 80 completely dissolved in 8 mL ultrapure water at 70 ˚C and then BIBF (50 mg) was added to form uniform BIBF-Sol.

2.4. Characterization of BIBF-NLCs-1 and BIBF-NLCs-2

2.4.1. Particle size and zeta potential

The particle size and size distribution of the two BIBF-NLCs were determined by dynamic light scattering (DLS) using a Malvern Particle Size Analyzer at room temperature. The zeta potential was detected by electrophoretic light scattering using the same equipment. Each value reported was the average of at least three measurements.

2.4.2. Transmission electron microscopy (TEM)

The morphology of the two BIBF-NLCs was examined using TEM (JEM-1200EX, Jeol, Japan). Samples were dropped onto a copper grid, stained with 2% phosphotungstic acid, and then air-dried before visualizing under TEM.

2.4.3. X-ray diffraction

BIBF, Blank-1, Blank-2, BIBF-NLCs-1 BIBF-NLCs-2 and physical mixtures were cured by lyophilization with sucrose as the lyoprotectant. The crystalline structures of BIBF within NLCs were determined with an X-ray diffractometer (D/Max-2400, Rigaku Corporation, Japan).

2.4.4. Fourier transform infrared spectroscopy (FT-IR)

Infrared spectra of BIBF, Blank-1, Blank-2, BIBF-NLCs-1 and BIBF-NLCs-2 were determined with a spectrometer (Bruker EQUINOX 55, Germany) over the wavelength range of 4000–400 cm^{-1} and with a

Table 1
Particle size, polydispersity index (PDI), zeta potential, drug loading (DL), and encapsulation efficiency (EE) of BIBF-NLCs-1 and BIBF-NLCs-2 (n = 3).

Formulation	Mean particle size (nm)	PDI	Zeta potential (mV)	DL (%)	EE (%)
BIBF-NLCs-1	142.70 ± 0.85	0.199 ± 0.002	+32.00 ± 0.50	2.28 ± 0.06	85.35 ± 2.94
BIBF-NLCs-2	7.99 ± 0.06	0.213 ± 0.018	+8.59 ± 0.46	2.08 ± 0.03	89.00 ± 3.45

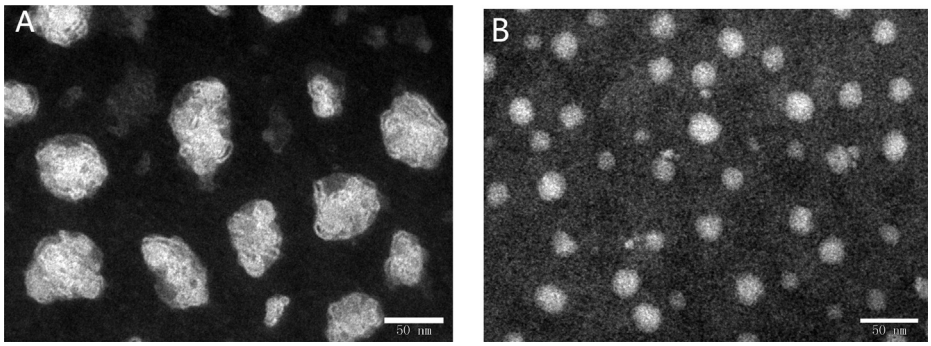

Fig. 1. TEM micrographs of (A) BIBF-NLCs-1 and (B) BIBF-NLCs-2; scale bar = 50 nm.

resolution of 4 cm^{-1}.

2.4.5. Drug loading and encapsulation efficiency

The drug loading (DL) and encapsulation efficiency (EE) of BIBF in the two BIBF-NLCs were determined by an ultrafiltration method.

Free BIBF was separated from the BIBF-NLCs-1 or BIBF-NLCs-2 by centrifugation using ultrafiltration tubes (MWCO: 30 kDa). The amount of BIBF in the filtrate and BIBF-NLCs-1 or BIBF-NLCs-2 was quantified by ultraviolet spectrophotometry (UV) at 385 nm. The calibration curve of absorbance against concentration of BIBF was A = 0.02579C-0.0207 (R^2 = 0.9992, where A = absorbance and C = BIBF concentration), RSD(%) values of both intraday and interday precision were less than 2%, the recovery rates of three different concentrations (low, medium and high) were all between 98.0% and 102.0%, with RSD(%) less than 2.0%.

The DL and EE were calculated according to the following formula (Ren et al., 2018):

$$\text{DL}\,(\%) = \frac{\text{Amount of BIBF in NLCs}}{\text{Amount of lipid} + \text{Amount of sufacant}} \times 100\%$$

$$\text{EE}\,(\%) = \frac{\text{Amount of BIBF in NLCs}}{\text{Amount of BIBF in NLCs} + \text{Free BIBF}} \times 100\%$$

2.5. Stability of BIBF-NLCs-1 and BIBF-NLCs-2

The stability of the two BIBF-NLCs was investigated in both simulated gastric fluid (pH1.2, SGF) and simulated intestinal fluid (pH6.8, SIF). A 1.5 mL BIBF-NLCs sample was mixed with 6 mL of SGF or SIF (containing 0.5% (w/v) Tween 80), and the mixtures were incubated at 37 °C for 6 h. At predetermined intervals, sample was removed for the measurement of particle size and distribution. Accordingly, the drug content was also determined.

2.6. In vitro release properties

The drug release of BIBF-Sol, BIBF-NLCs-1 and BIBF-NLCs-2 was determined using a dialysis membrane (MWCO: 8000–14,000) in SGF or SIF (containing 0.5% (w/v) Tween 80 to reach sink conditions). The experiment was conducted in an incubator shaker set at 37 ± 0.5 °C with a shaking speed of 100 rpm. At predetermined intervals, samples were removed and determined by UV spectroscopy at 385 nm.

2.7. Cell evaluation

2.7.1. Cell uptake investigation

The cell uptake of BIBF-Sol, BIBF-NLCs-1 and BIBF-NLCs-2 was analyzed by confocal microscopy (LSM 710 NLO, Zeiss, Germany) and flow cytometry (BD FACSAria™ III, BD Biosciences, Shanghai, China). Coumarin-6 (C6) was used in place of BIBF as a fluorescent probe.

The confocal dedicated circular glass piece was placed in advance in a 24-well plate. Caco-2 cells were then seeded in the 24-well plates and adhered for 24 h until confluent. The cells were then incubated with C6 loaded NLCs (C6-NLCs-1 or C6-NLCs-2) or solution with a C6 concentration of 8 μg/mL (C6-Sol) for 0.5 h and 2 h. The control group was an equal amount of high glucose DMEM medium incubated for the same time. The cell nucleus was stained with DAPI. At each time point, the sample was imaged by confocal microscopy.

Cellular uptake was quantified using a flow cytometry system. Caco-2 cells were seeded in a 12-well plate and cultured for 24 h until confluent. The same C6 concentration, group, and incubation times were analyzed as for the confocal microscopy. At each time point, the mean intracellular fluorescence intensity was measured by flow cytometry system (FCS) analysis.

2.7.2. Transport of drugs in Caco-2 monolayers

The Caco-2 monolayers were established by Transwell (Cat. No. 3401, Corning Costar® Corporation, Cambridge, MA, USA). Caco-2 cells were seeded on polycarbonate filters (0.4 μm pore size, 1.13 cm^2 growth area) inside cell culture chambers. After being cultured for 18–21 days, the fluorescein sodium leakage rate experiment (Varadi et al., 2017) was carried out to verify the successful establishment of the Caco-2 cell monolayer model.

Transport studies of BIBF-Sol, BIBF-NLCs-1 and BIBF-NLCs-2 were performed as previously described (Hubatsch et al., 2007) with slight modifications. The culture medium was replaced by transport medium (Hank's balanced salt solution, HBSS) and equilibrating at 37 °C for 15 min. After discarding the transport medium, 0.5 mL of BIBF-Sol, BIBF-NLCs-1 or BIBF-NLCs-2 (20 μg/mL of BIBF equivalent) in HBSS and 1.5 mL of fresh HBSS solution, which were prewarmed to 37 °C, were applied to the apical side and the basolateral side respectively. The receiver medium in the basolateral side was collected and then completely replaced by 1.5 mL of fresh HBSS solution after 0.25, 0.5, 1, 2 and 4 h. Methanol was added to the samples, followed by vortexing and centrifuging, then the supernatants were measured by HPLC at 385 nm to determine the amount of drug transported.

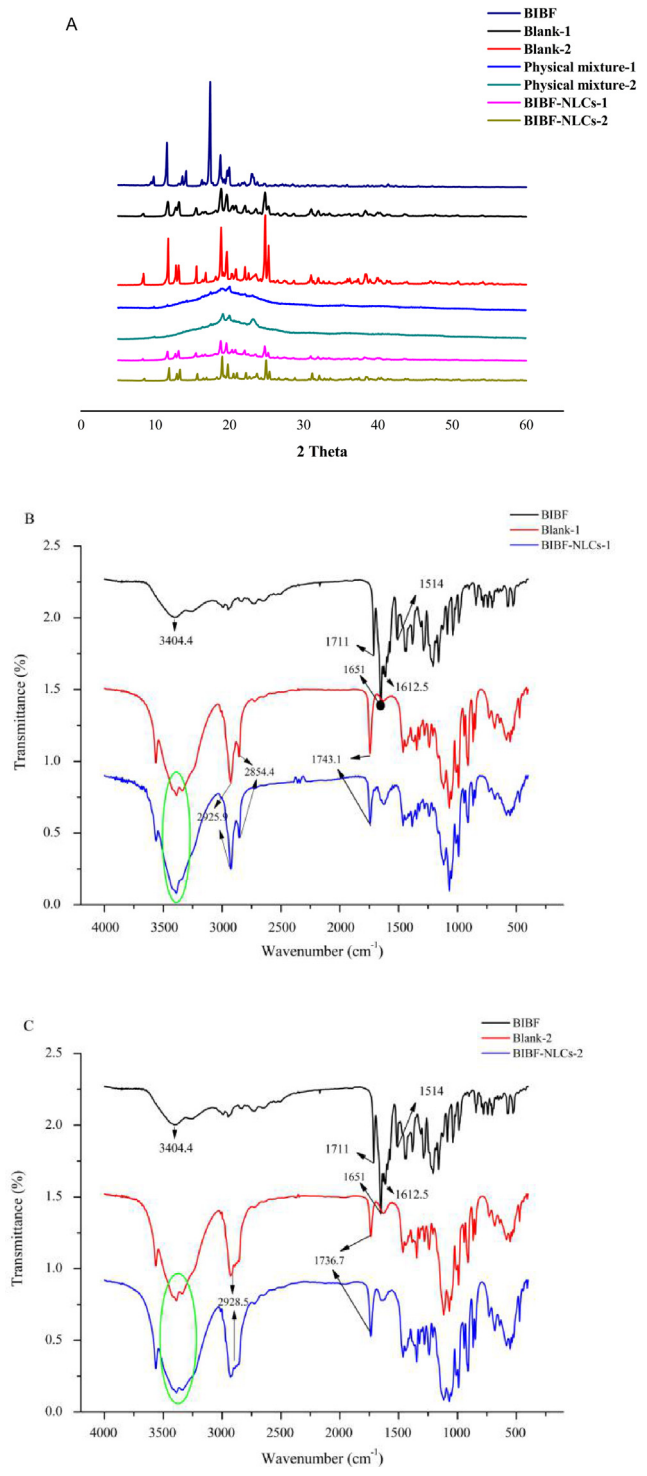

Fig. 2. (A) X-ray diffractions and (B, C) FT-IR of BIBF, Blank-1, Blank-2, BIBF-NLCs-1 and BIBF-NLCs-2. 1.

2.8. In vivo pharmacokinetic study

Twenty-five SD rats were randomly divided into five groups: BIBF-Sol (iv, 10 mg/kg), BIBF-Sol (po, 30 mg/kg), BIBF-NLCs-1 (po, 30 mg/kg), BIBF-NLCs-2 (po, 30 mg/kg) and solid dispersion of BIBF (BIBF-SD) (po, 30 mg/kg). The BIBF-SD used in this study was prepared by hot melt extrusion using a twin-screw extruder (ZE-014, ATS Engineering Limited, China). Tannic acid and PVP-VA64 (BIBF/tannic acid/PVP-VA64 = 2/2/6) was used as the carrier materials. The specific parameters were as follows: 35 rpm was the extrusion speed, and the extrusion temperatures in different regions were set as 153 ˚C, 153 ˚C, 150 ˚C, 150 ˚C, 130 ˚C, 130 ˚C and room temperature from front to back.

Blood samples were collected into centrifuge tubes from the orbital vein at 0.5, 1, 2, 4, 6, 8, 10, 12 and 24 h after oral administration. For intravenous administration, blood was taken at 0.083, 0.25, 0.5, 1, 2, 4, 8, 10, 12 and 24 h after administration. The concentration of BIBF in the plasma samples was determined by ultrahigh performance liquid chromatography tandem mass spectrometry (UPLC-MS/MS). Ethyl acetate was used as the extractant and piperine was used as an internal standard (IS). The method of UPLC/MS/MS was as follow: An ACQUITY™ UPLC system (Waters Corp., Milford, MA, USA) and Thermo C18 column (50 mm × 2.1 mm ID, 1.7 μm) was used, with a gradient elution of acetonitrile and a 0.1% formic acid solution (70:30). Mass spectrometric determination was performed in positive ESI mode, and the compounds were quantified by multiple reaction monitoring (MRM) of the transitions of m/z 540.27 → 113.05 for BIBF and m/z 286.16 → 115.07 for IS, respectively. The standard curve for BIBF was y = 0.0227x − 0.0261, showed good linearity with correlation coefficient of 0.9936.

The relative bioavailability (F_{rb}) and absolute bioavailability (F_{ab}) were calculated as follows(Ren et al., 2018):

$$F_{rb} = \frac{AUC_{po} \times Dose_{po-sol}}{AUC_{po-sol} \times Dose_{po}}$$

$$F_{ab} = \frac{AUC_{po} \times Dose_{iv}}{AUC_{iv} \times Dose_{po}}$$

where AUC_{po} and $Dose_{po}$ represent the area under the curve and the dose of the oral formulations. $AUC_{sol\text{-}po}$ and AUC_{iv} represent the areas under the curve of the BIBF-Sol given orally and intravenously, respectively; $Dose_{sol\text{-}po}$ and $Dose_{iv}$ represents the doses of BIBF-Sol given orally and intravenously, respectively.

2.9. In vivo antitumor effect

Homemade BIBF soft capsules (BIBF-SCs) were prepared according to the prescription of the commercially available Ofev®. Together with BIBF-NLCs-1 and BIBF-NLCs-2, the antitumor effects of BIBF-SCs after oral administration were investigated in a subcutaneous LLC xenograft model of murine lung carcinoma.

C57BL/6 mice were injected subcutaneously into the right axillary area with LLC cells. When the tumor size reached 80–120 mm^3, the mice were randomly divided into 5 groups (n = 5): Control (ultrapure water), BIBF-Sol (po, 45 mg/kg), BIBF-NLCs-1 (po, 45 mg/kg), BIBF-NLCs-2 (po, 45 mg/kg), BIBF-SCs (po, 45 mg/kg). The mice were administered orally with the above drugs once every two days for 8 times in total. Body weight and tumor size were recorded before each dose, and the first dose was considered as day 1. The length of the major axis (a) and minor axis (b) of the tumor were measured using vernier calipers, and the tumor volume was calculated by the equation of $v = 1/2 \times a \times b^2$. On the fifteenth day, mice of each group were sequentially sacrificed, and the tumors were excised and weighed.

2.10. Gastrointestinal irritancy and liver damage

Fifty C57BL/6 mice were divided into 5 groups: Control (ultrapure water), BIBF-Sol (po, 60 mg/kg), BIBF-NLCs-1 (po, 60 mg/kg), BIBF-NLCs-2 (po, 60 mg/kg), BIBF-SCs (po, 60 mg/kg), with oral administration four times a week for one week. At the end of administration, a 1.0 mL blood sample was collected from the eyeball. The contents of alanine aminotransferase (ALT) and aspartate aminotransferase (AST) in plasma were measured using a microplate reader. Subsequently, the mice in each group were sequentially sacrificed. The stomach, duodenum, jejunum and ileum were removed, fixed and stained, then observed under the microscope.

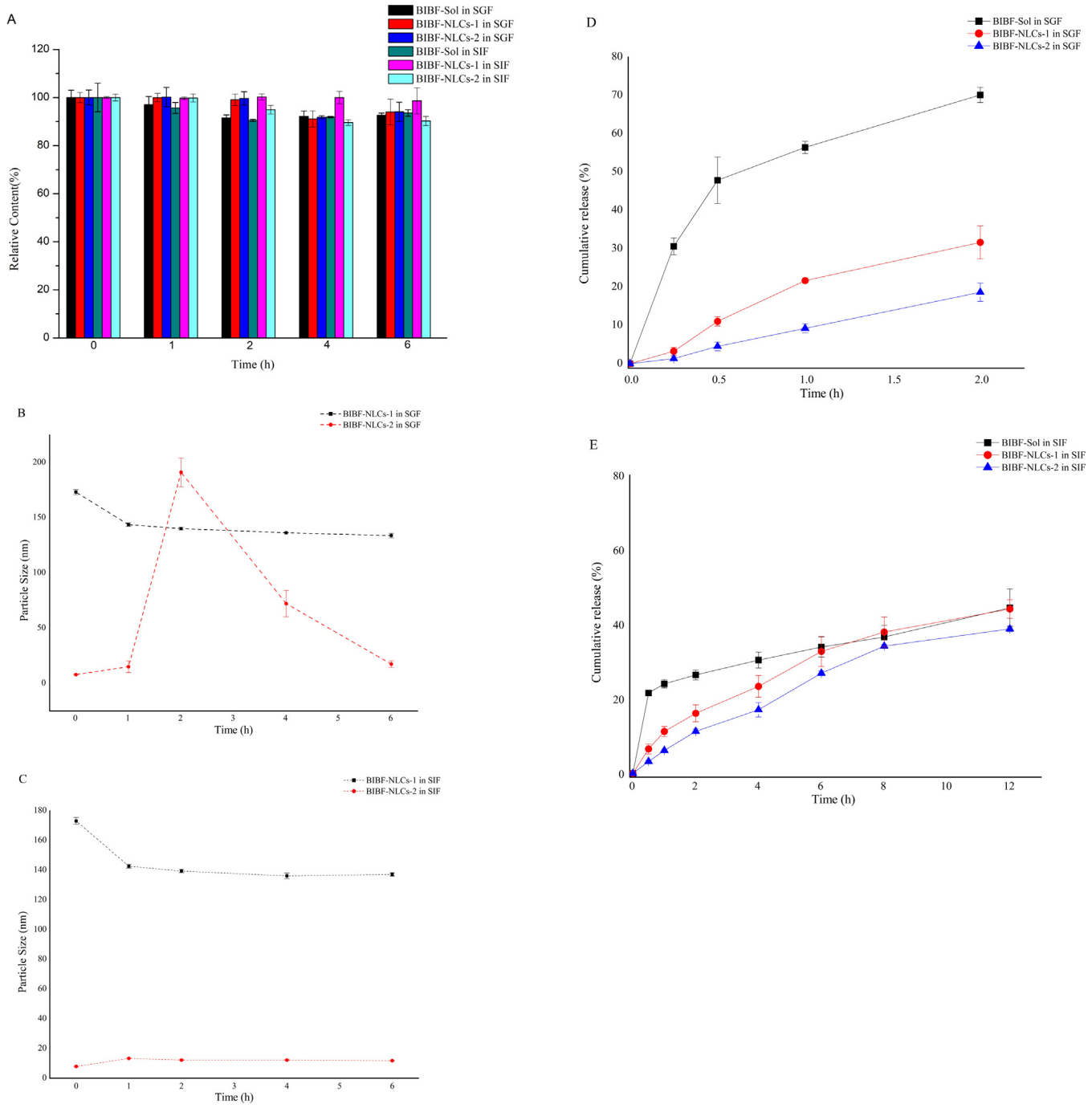

Fig. 3. (A) Content change, (B, C) Particle size variation and (D, E) Cumulative release of BIBF-NLCs-1 and BIBF-NLCs-2 in SGF (pH = 1.2) and SIF (pH = 6.8, containing 0.5% (w/v) Tween 80).

2.11. Statistical analysis

The pharmacokinetic parameters were calculated using DAS 2.0 software.

All data was presented as mean ± SD, and a *t*-test was used for statistical analysis. A p value of < 0.05 was considered as a statistical difference and a p value of < 0.01 was considered as a significant statistical difference.

3. Results

3.1. Characterization of BIBF-NLCs-1 and BIBF-NLCs-2

The DL, EE, particle size and zeta potential of BIBF-NLCs-1 and BIBF-NLCs-2 were determined and are summarized in Table 1. The two BIBF-NLCs had similar DL and EE. As shown in Table 1, BIBF-NLCs-1 showed a uniform particle size of 142.70 ± 0.85 nm, while BIBF-NLCs-2 showed a much smaller particle size of 7.99 ± 0.06 nm. And they exhibited a positive zeta-potential of + 32.00 ± 0.50 mV and + 8.59 ± 0.46 mV, respectively.

TEM micrographs are shown in Fig. 1. It can be seen that they showed a near spherical or spherical morphology. BIBF-NLCs-1 and

Table 2
Models for drug-release fitting and correlation coefficients of BIBF-NLCs-1 and BIBF-NLCs-2 in SGF (pH = 1.2) and SIF (pH = 6.8, containing 0.5% (w/v) Tween 80).

Preparations	Release medium	Model	Equation	R^2
NLCs-1	SGF	Zero-order	$Q = 1.8303t + 22.6697$	0.4379
		First-order	$Q = 51.6717*(1 - \exp(-0.4686t))$	0.9970
		Higuchi	$Q = 15.2133t^{1/2} + 0.0694$	0.8475
	SIF	Zero-order	$Q = 3.3837t + 5.5645$	0.9803
		First-order	$Q = 209.5520*(1 - \exp(-0.0220t))$	0.9601
		Higuchi	$Q = 11.6363t^{1/2} - 7.4994$	0.9106
NLCs-2	SGF	Zero-order	$Q = 2.6294t + 14.9857$	0.6196
		First-order	$Q = 63.5050*(1 - \exp(-0.2032\ t))$	0.9552
		Higuchi	$Q = 11.6026t^{1/2} + 10.1754$	0.7626
	SIF	Zero-order	$Q = 3.8489t + 0.3856$	0.9776
		First-order	$Q = 49.5551*(1 - \exp(-0.1127\ t))$	0.9914
		Higuchi	$Q = 20.6072\ t^{1/2} - 20.2325$	0.8687

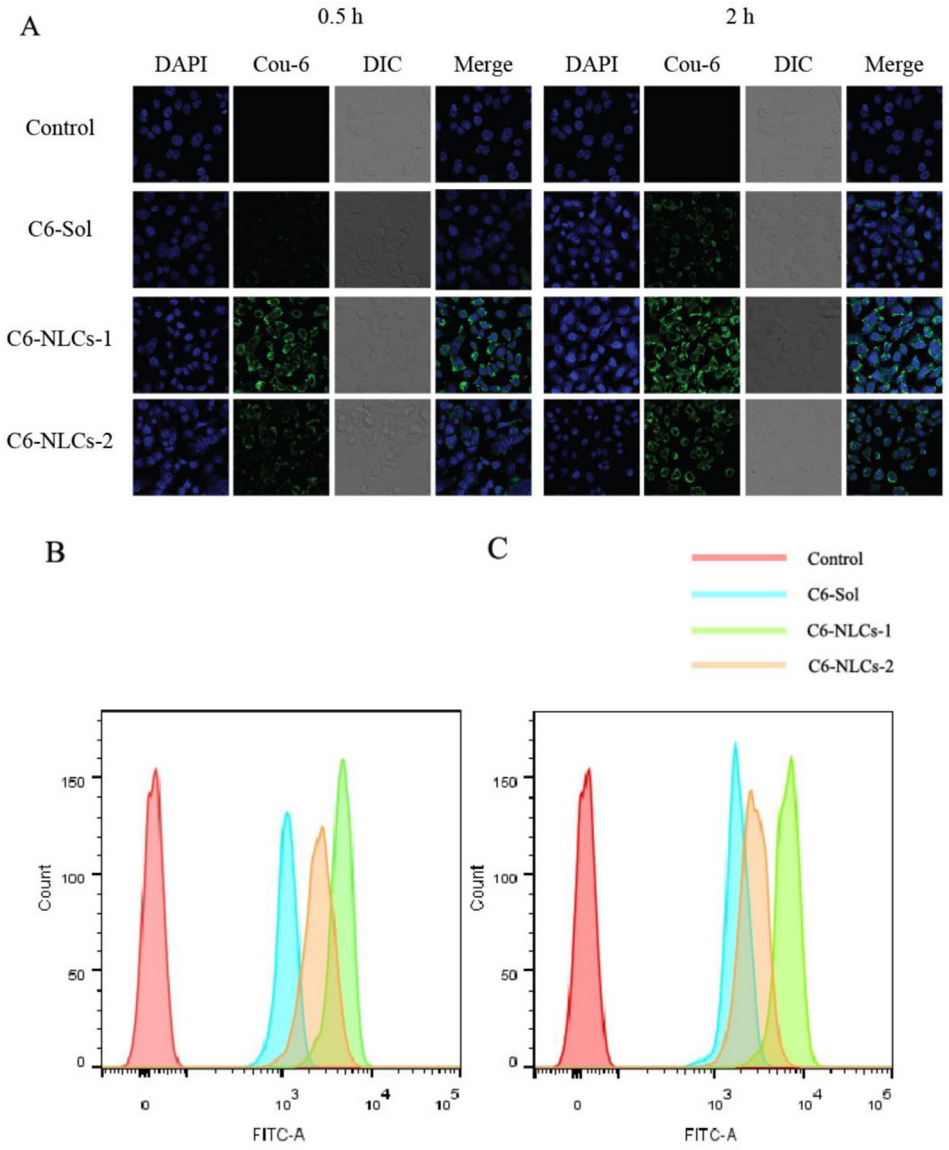

Fig. 4. (A) The CLSM images, (B, C, D) Flow cytometry analysis of the cellular uptake of C6-sol, C6-NLCs-1 and C6-NLCs-2 by caco-2 cell monolayer for 0.5 h and 2 h, (E) Cumulative amount of transported BIBF through caco-2 monolayers at different time and (F) Papp of BIBF from different formulations at 4 h. (**$p < 0.01$, *$p < 0.05$, compared to BIBF-Sol; ##$p < 0.01$, compared to BIBF-NLCs-2).

BIBF-NLCs-2 both showed a homogeneous size distribution, which validated the particle size data provided by DLS in Table 1. The particle size determined by TEM was smaller than by DLS due to the dehydration of the samples with TEM.

The results of XRD analysis are shown in Fig. 2A. It can be seen that the characteristic diffraction peaks of BIBF disappeared in the two BIBF-NLCs, and only characteristic diffraction peaks similar to Blank-1 and Blank-2 can be seen. This confirms that the BIBF was almost completely

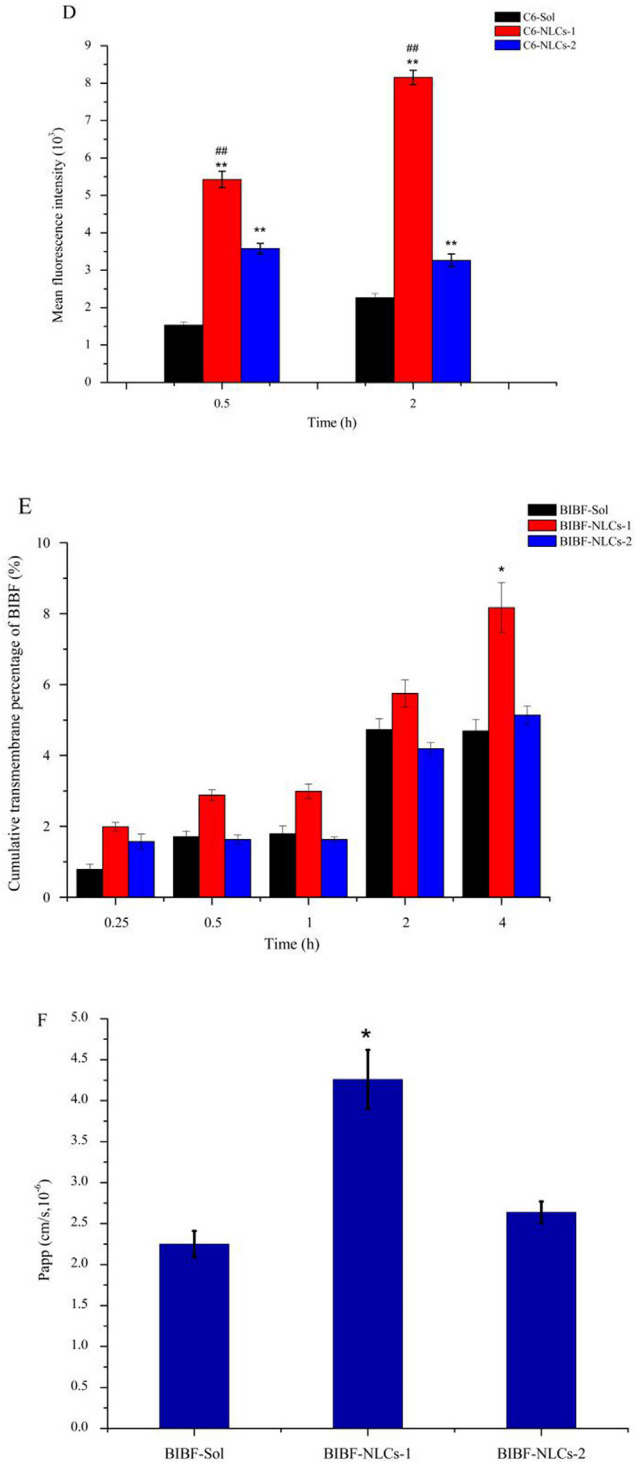

Fig. 4. (*continued*)

entrapped within the NLCs and existed in an amorphous form, which should aid in improving the absorption rate and bioavailability (Shah et al., 2016).

As shown in Fig. 2B and C, the infrared spectrum of BIBF showed characteristic peaks of the carbonyl (C═O) from its unique tertiary and secondary amides at 1651 cm^{-1} and 1612.5 cm^{-1}, respectively, and a characteristic peak of C═O from the benzyl ester at 1711 cm^{-1}. In the infrared spectra of Blank-1, Blank-2, BIBF-NLCs-1 and BIBF-NLCs-2, it was observed that several C═O characteristic peaks of BIBF disappeared. The C═O characteristic peak of the saturated ester group from long-chain fatty acid ester appeared at 1743.1 cm^{-1} or

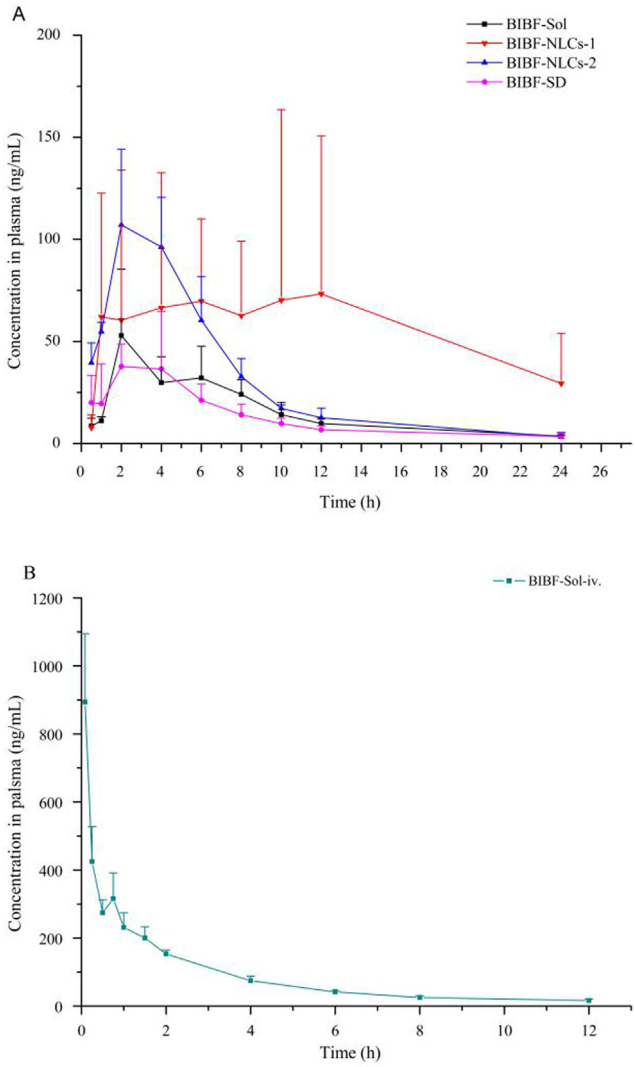

Fig. 5. (A) The mean plasma concentration time curves of BIBF after a single dose of 30 mg/kg oral administration of BIBF-Sol, BIBF-NLCs-1, BIBF-NLCs-2, BIBF-SD and (B) 10 mg/kg intravenous injection of BIBF-Sol. (n = 5).

1736.7 cm^{-1}, and the characteristic peak of alkyl groups appeared near 2925 cm^{-1}. In addition, a hydroxyl (−OH) characteristic peak of the protective agent sucrose was observed at around 3400 cm^{-1}. This further demonstrated that BIBF was completely encapsulated inside the NLCs.

3.2. Stability of BIBF-NLCs-1 and BIBF-NLCs-2 in SGF and SIF

As shown in Fig. 3A, the drug content of BIBF-NLCs-1 and BIBF-NLCs-2 remained almost unchanged at 100% during incubation for 2 h in SGF. By extending the time to 6 h, the drug content of the two BIBF-NLCs still remained above 94%. However, the drug content of BIBF-NLCs-2 incubated for 6 h in SIF decreased by nearly 10%, with an onset around the second hour. When considering drug content, BIBF-NLCs-1 showed improved protection for the drugs in the intestinal environment. From the change in particle size (Fig. 3B and C), only BIBF-NLCs-2 showed significant changes during SGF incubation, the particle size increased from 7.88 ± 0.26 nm to 191.00 ± 13.02 nm after 2 h and then decreased to 17.14 ± 3.02 nm after 6 h, which indicated that the acid resistance of BIBF-NLCs-2 was relatively weak. The decline in drug content and the appearance of aggregation may be related to its large relative surface area and low surface potential.

Table 3
Pharmacokinetic parameters of BIBF-Sol, BIBF-NLCs-1, BIBF-NLCs-2, BIBF-SD after oral administration and BIBF-Sol after intravenous injection (n = 5).

Parameter	Unit	BIBF-Sol	BIBF-NLCs-1	BIBF-NLCs-2	BIBF-SD	BIBF iv.
$t_{1/2z}$	h	3.72 ± 1.68	7.06 ± 7.91	3.51 ± 0.62	8.69 ± 4.97	2.41 ± 0.32
$AUC_{(0-t)}$	μg/L·h	311.04 ± 99.45	972.96 ± 296.60	742.35 ± 155.57	315.91 ± 128.80	1108.84 ± 76.05
$AUC_{(0-\infty)}$	μg/L·h	409.29 ± 64.98	1376.96 ± 479.18	752.35 ± 145.40	360.37 ± 135.89	1138.02 ± 79.88
C_{max}	ug/L	68.81 ± 22.59	113.54 ± 77.77	108.17 ± 35.23	45.46 ± 21.31	893.56 ± 200.71
F_{rb}	%	–	312.81	238.67	101.57	–
F_{ab}	%	9.35	29.25	22.32	9.50	100

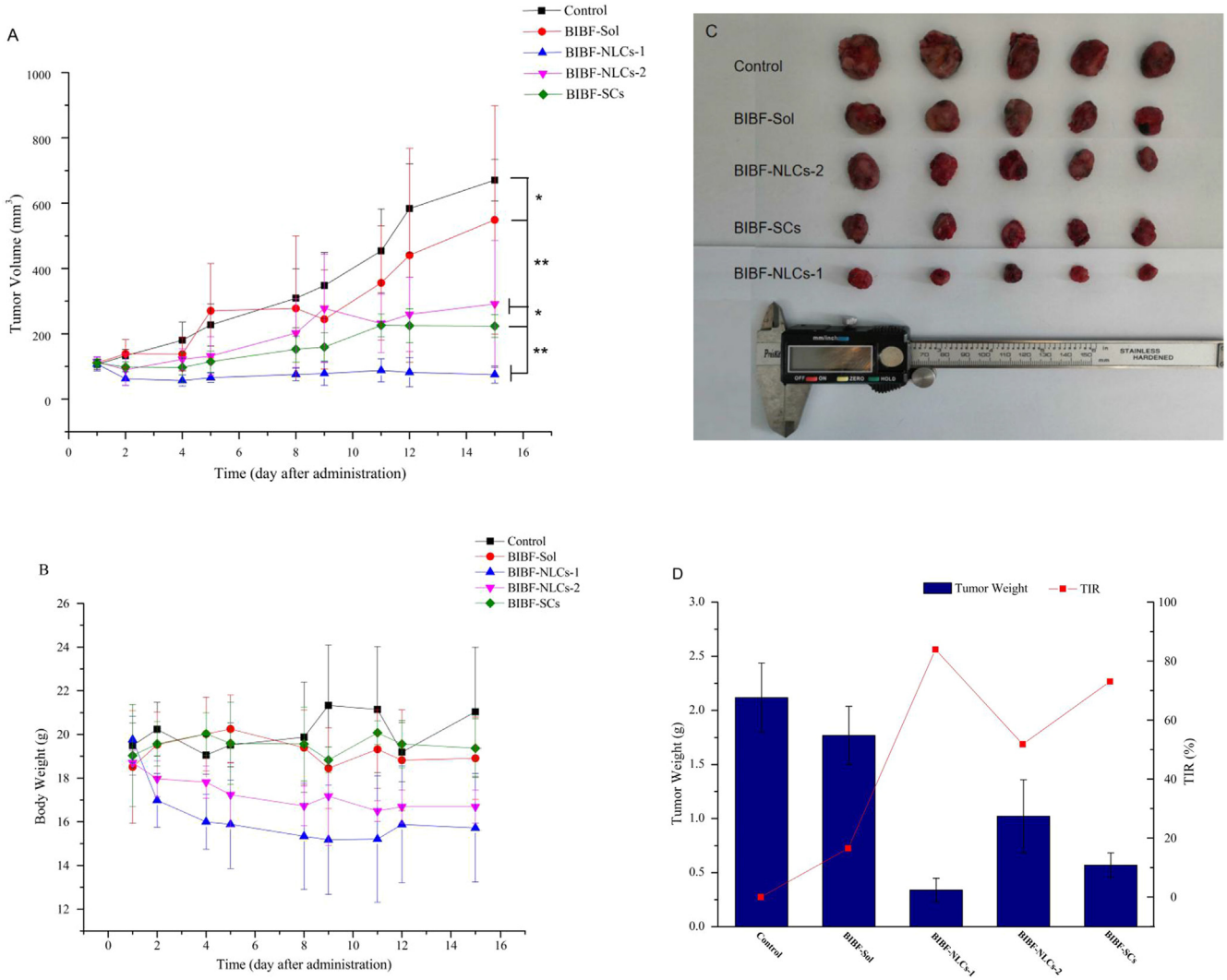

Fig. 6. (A) Tumor volume, (B) body weight changes, (C) photographs of the tumors, (D) tumor weight and TIR (%) of Lewis-bearing mice treated with oral of distilled water (Control), BIBF-Sol, BIBF-NLCs-1, BIBF-NLCs-2 and BIBF-SCs. Data represent the mean ± standard deviation (n = 5). (*p < 0.05; ** p < 0.01).

3.3. In vitro release of BIBF-NLCs-1 and BIBF-NLCs-2

The drug release properties in SGF or SIF (containing 0.5% (w/v) Tween 80) are shown in Fig. 3D and E. Compared to BIBF-Sol, BIBF-NLCs could achieve sustained release characteristics and reduce the drug burst release to some extent. This suggested that the drug was mainly present in the interior of the NLCs, with minimal surface distribution. Only as the lipid structure was gradually destroyed could the drug be released.

In order to investigate the drug-release kinetics, the data obtained from the *in vitro* release studies of BIBF-NLCs were treated according to Zero-order (fraction drug release *vs.* time), first-order (log cumulative percentage of drug remaining *vs.* time) and Higuchi's (fraction drug release *vs.* square root of time) model equations to interpret mechanism and kinetics of drug release. As shown in Table 2, the *in vitro* release profiles of BIBF from NLCs-1 in SGF and NLCs-2 in SGF and SIF followed the first-order release kinetics with R^2 = 0.9970, 0.9552 and 0.9914, respectively. This indicated that most of the liquid lipid was distributed in the solid lipid core, and the drug incorporated into the solid–liquid lipid matrix was released in a sustained manner via erosion or degradation. Besides, the *in vitro* release profiles of BIBF from NLCs-1 in SIF followed the zero-order release kinetics with R^2 = 0.9803, the mechanism for which might be explained by the fact that the rate of drug release was independent of drug concentration (Cheewatanakornkool et al., 2017; Iqbal et al., 2014; Pradhan et al., 2015; Zhang et al., 2013).

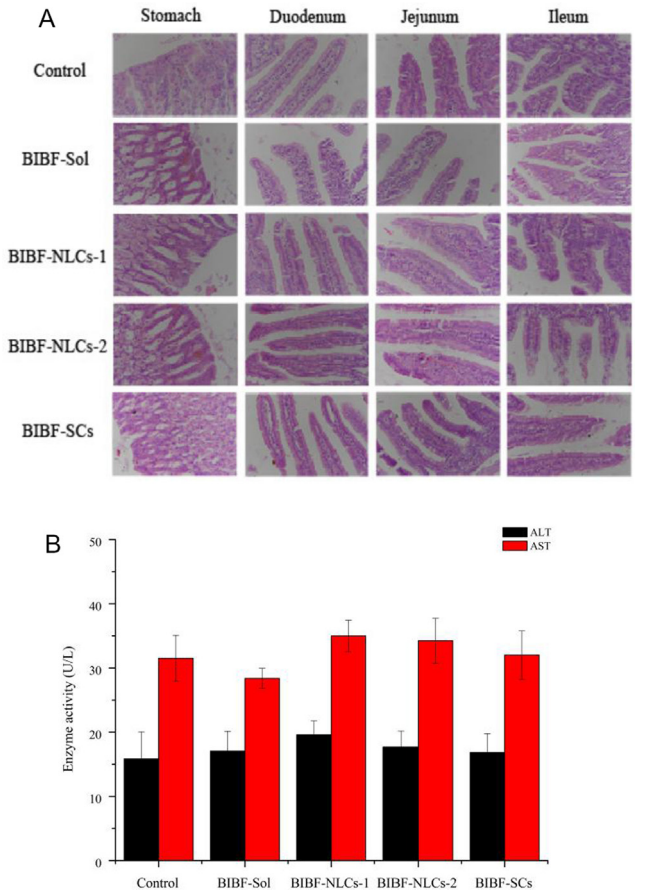

Fig. 7. (A) Images of gastrointestinal irritation of BIBF-Sol, BIBF-NLCs-1, BIBF-NLCs-2 and BIBF-SCs and (B) Enzyme activity of ALT and AST in plasma of mice in each group (n = 3).

3.4. Cell evaluation

3.4.1. Cell uptake investigation

It could be seen from Fig. 4A that the fluorescence intensity of C6 after 2 h incubation was stronger than 0.5 h, indicating that at the concentration employed, cellular uptake of C6-Sol, C6-NLCs-1 and C6-NLCs-2 was time-dependent. This is consistent with the results reported by Harush-Frenkel et al. (2008). In addition, the fluorescence intensity of C6 in Caco-2 cells treated with C6-NLCs-1 and C6-NLCs-2 was stronger than that of C6-Sol, both at 2 h or 0.5 h. From this, it can be speculated that these two strategies are beneficial for the absorption of the drug in the intestine.

To further confirm the internalization behavior and quantitative cellular uptake, flow cytometry experiments were performed. As shown in Fig. 4B–D, the average fluorescence intensity of C6 uptake by the C6-NLCs-1 group was significantly higher than that of the C6-NLCs-2 and C6-Sol groups. At 0.5 h and 2 h, the mean fluorescence intensity in the C6-NLCs-1 group was approximately 1.5-fold and 2.5-fold of that of C6-NLCs-2 group, respectively, which was approximately 3.5-fold and 3.6-fold of that in C6-Sol group. Combining the results of both experiments, C6-NLCs-1 enhanced the ability to be taken up by Caco-2 cells.

3.4.2. Transport of drugs in caco-2 monolayer

In this study, the successful establishment of the caco-2 cell monolayer model was verified through the fluorescein sodium leakage rate experiment (Marzin et al., 2018) (Papp = (5.74 ± 0.31) × 10^{-7} cm/s). As shown in Fig. 4E and F, at the different time points, the transmembrane amount of BIBF-NLCs-1 showed a significant increase compared to both BIBF-NLCs-2 and BIBF-Sol, which further confirmed the results above (Fig. 4A–D). The Papp of BIBF-NLCs-1 at 4 h was (4.26 ± 0.36) × 10^{-6} cm/s, which was 1.61-fold of BIBF-NLCs-2 and 1.89-fold of BIBF-Sol, respectively.

3.5. In vivo pharmacokinetic study

The BIBF mean plasma concentration time curves are illustrated in Fig. 5 and the detailed pharmacokinetic parameters are shown in Table 3. According to Table 3, the F_{ab} of oral BIBF-Sol in rat was only 9.35%, while the F_{ab} of BIBF-NLCs-1 and BIBF-NLCs-2 was significantly increased to 29.25% and 22.32%, respectively. This was an exciting result, and they both had a competitive $AUC_{(0-t)}$, which was approximately 3.13-fold and 2.39-fold that of the oral BIBF-Sol group. It also can be seen that the bioavailability of BIBF-SD was barely improved.

3.6. In vivo antitumor effect

The tumor growth and tumor images from the 5 groups of mice are shown in Fig. 6A–C. The tumor weight and tumor inhibition rate (TIR) is shown in Fig. 6D. As shown in Fig. 6A, tumor volume was BIBF-NLCs-1 < BIBF-SCs < BIBF-NLCs-2 < BIBF-sol < control group. The control group showed 670.75 ± 63.44 mm^3 tumor volume, and the tumor volume of BIBF-sol group was 548.90 ± 349.79 mm^3, which showed a significant advantage compared to the control group ($p < 0.05$). The tumor volume of BIBF-NLCs-2, BIBF-SCs and BIBI-NLCs-1 group was 291.53 ± 194.43 mm^3, 223.86 ± 34.70 mm^3 and 75.15 ± 25.78 mm^3, respectively, which all showed extremely significant differences compared to the control group ($p < 0.01$). BIBF-NLCs-2 showed a similar tumor suppression to BIBF-SCs, which significantly slowed tumor growth. It is worth noting that BIBF-NLCs-1 showed extremely significant differences compared to all the other groups ($p < 0.01$). Furthermore, the results of tumor weight and TIR (%) changed in different groups confirmed that BIBF-NLCs-1 showed excellent anti-tumor effects and could almost completely inhibit tumor growth in the early stages, with a tumor weight and TIR (%) reaching 2.12 ± 0.32 g and 83.93% compared to 0.34 ± 0.11 g and 0 of control group.

3.7. Gastrointestinal irritancy and liver damage

Clinic Study showed that BIBF could lead to a significant increase in gastrointestinal side effects, such as loss of appetite and liver damage. To verify this conjecture, gastrointestinal irritation and liver damage experiments were performed. The image of gastrointestinal irritation sections is shown in Fig. 7A. Among the three mice observed in each group in parallel, only one of the mice in the BIBF-Sol group and one in BIBF-SCs group showed mild edema of the stomach. This indicated that BIBF-NLCs-1 and BIBF-NLCs-2 did not increase gastrointestinal irritation, because BIBF was wrapped in NLCs. Liver damage is indicated by the enzyme activity of ALT and AST in blood plasma(Gurung et al., 2013; Yanagiba et al., 2016) (Fig. 7B). As shown in Fig. 7B, compared with the control group, the enzyme activities of ALT and AST in the plasma of the other groups fluctuated, but no significant differences ($p > 0.05$) were observed.

4. Discussion

The purpose of this study was to improve the intestinal absorption of BIBF with NLCs as a drug delivery vehicle, and further improve its oral bioavailability. In the field of oral drug delivery systems, it must be ensured that the drug contained in the NLCs is stable in the stomach and gastrointestinal environments. The good stability exhibited by the NLCs structure can increase the stability of the drug within, which plays a crucial role in the absorption of drugs. Some reports have shown that BIBF is easily degraded in PBS buffered saline. When incubated in PBS with pH 7.4 for 4 h, the degradation rate reached 80% (Vaidya et al.,

2019). Therefore, in this study, the stability of BIBF-NLCs was examined in SGF and SIF. Drug content and particle size were used as the two main parameters to evaluate the stability of BIBF-NLCs in the gastrointestinal environment. According to the results of Fig. 3, it can be seen that BIBF-NLCs-1 and BIBF-NLCs-2 had good content stability in gastrointestinal. The particle size of BIBF-NLCs-2 first increased and then decreased, which can be explained based on the aggregation due to its large relative surface area and low surface potential. The aggregated particles gradually increases until they can be filtered out by 0.45 μm needle filter. In addition, it released less in SGF and SIF. This ensured that the BIBF-NLCs were in contact with the intestinal epithelium and mucosa mostly in the form of the lipid carrier, avoiding the efflux of BIBF by P-gp, increasing the amount of drug taken up by the intestinal cells, and improving absorption in the intestine (Beloqui et al., 2016b).

In cytological studies, BIBF-NLCs-1 exhibited unique advantages in simulated intestinal uptake and transmembrane processes. It has long been believed that particle size plays a crucial role in the process of cell internalization, and that generally a small size is more favorable for entry into cells. However, in the present study, the opposite was observed, whereby the internalization of small-sized BIBF-NLCs-2 by caco-2 cells was inferior to that of BIBF-NLCs-1, which had the relatively larger particle size. Some recent studies (Kulkarni and Feng, 2013) have concluded that a too small particle size may adversely affect endocytosis of the nanoparticle (NP) by cells, as the surface capabilities of small NPs may not be sufficient to achieve the desired binding energy during endocytosis. Moreover, after entering the systemic circulation, the blood clearance rate of smaller NPs (< 80 nm) is relatively high, while the particles under 200 nm in diameter might be more similar to low density lipoprotein (LDL) and easier to escape from recognition by the reticuloendothelial system, thus attained an extended circulation time as compared with those of a larger diameter(Kulkarni and Feng, 2013).

On the other hand, the particle shape, particle size, material properties (such as compressibility of materials) and surface chemistry of NLCs will affect the means and extent of nanomedicine cell entry (Beloqui et al., 2016a; Sahay et al., 2010). According to previous studies (Ren et al., 2018), due to the negative charge of the cell membrane, it is generally believed that positively charged NPs should improve internalization compared to the negative ones. Positively charged particles can interact with negatively charged extracellular proteoglycans, achieving high affinity for intestinal epithelial cells. Normally, positively charged particles are primarily internalized into cells through clathrin-mediated endocytosis (CME), while negatively charged particles enter the cell mainly through caveolae-mediated endocytosis (Iqbal et al., 2012; Sahay et al., 2010). Based on the results of this study, it can be inferred that a relatively high positive surface potential may be more advantageous for internalization of NLCs into cells.

In the pharmacokinetic study, BIBF-NLCs-1 and BIBF-NLCs-2 significantly improved the bioavailability of BIBF, while BIBF-SD had little effect. It indicated that in this case, the solid dispersion strategy that merely solved the dissolution problem of BIBF was ineffective in improving its bioavailability *in vivo*. The reason for this result was that BIBF-SD was not able to alleviate the efflux of BIBF by P-gp during its oral administration, which further led to minimal improvement in intestinal absorption.

At the same time, it was worth noting that, BIBF-NLCs-1 was better than BIBF-NLCs-2 in oral bioavailability, and distinctions between them were observed from the *in vitro* release and cell results. And the oral bioavailability of BIBF-NLCs-2 was much better than BIBF solution. This can be attributed to the following two aspects. First, according to the stability study of BIBF-NLCs-2 (Fig. 3A, B and C), it can be inferred that in the intestinal environment of rats, small particles were agglomerated due to their large specific surface area and low surface potential, which resulted in an increase in particle size. The insufficient bending energy during the endocytic process caused by the small particle size was therefore somewhat relieved. The particles agglomerated by BIBF-NLCs-2 would possibly be taken up by more clathrin-mediated endocytic pathways due to identifying as particles with the appropriate size. Second, this may be due to another mechanism of NLCs absorption in the small intestine. After the NLCs reached the intestine, the lipid components were gradually degraded by local enzymes, leading to the formation of mixed micelles together with bile salts. These could then be captured and absorbed by intestinal cells in the form of mixed micelles (Beloqui et al., 2017).

The results of gastrointestinal irritation and liver damage experiments showed that during the experimental time frame, the gastrointestinal irritation was alleviated and no liver damage was caused by the preparations in the mice. These non-invasive carriers increasing intestinal cellar uptake and improving absorption without impairing the function of the intestinal epithelial mucosa. This indicated that the weight loss of BIBF-NLCs-1 and BIBF-NLCs-2 mice was not caused by gastrointestinal irritation, but may be due to other reasons such as decreased appetite caused by oral gavage.

BIBF-NLCs-1 exhibited excellent anti-tumor effect, which may be attributed to the following points. Firstly, the excellent zeta potential (+32.9 mV) made NLCs more stable, which was also reflected in the stability in the gastrointestinal tract. BIBF was stably encapsulated in the inner core, preventing it from losing activity prematurely during transport, and thereby increasing accumulation in the tumor area. Secondly, the solid lipid used in the formulation, glyceryl monooleate, has certain adhesion properties on the intestinal mucosa (Liu et al., 2011). This is beneficial for prolonged retention of NLCs in the intestine, and therefore prolonged contact with the intestinal mucosa, which can facilitate the continuous absorption of BIBF-NLCs-1 in the intestine. It has been reported (Bekaii-Saab and Villalona-Calero, 2005) that the antitumor activity of the drug is related to the exposure time, so the reservoir effect of NLCs was favorable.

5. Conclusions

In summary, the oral bioavailability of BIBF is successfully increased using a nanostructured lipid carrier as the delivery vector, achieved by reducing P-gp efflux and improving intestinal absorption. The two BIBF-NLCs may reduce the intestinal irritation of BIBF and not cause an increase in liver toxicity. Besides, *in vivo* anti-tumor efficiency study in mice bearing LLC lung tumor indicated that BIBF-NLCs-1 and BIBF-NLCs-2 had excellent tumor inhibition. The results of this study were encouraging for further development of nanotechnology approaches in the field of oral small molecule targeted drugs.

CRediT authorship contribution statement

Yunjing Zhu: Data curation, Formal analysis, Investigation, Writing - original draft, Writing - review & editing. **Xue Liang:** Data curation, Formal analysis, Investigation, Writing - original draft, Writing - review & editing. **Cong Lu:** Investigation, Formal analysis. **Yihan Kong:** Investigation, Formal analysis. **Xing Tang:** Resources. **Yu Zhang:** Writing - review & editing, Visualization. **Tian Yin:** Writing - review & editing, Visualization. **Jingxin Gou:** Writing - review & editing, Visualization. **Yanjiao Wang:** Writing - review & editing, Visualization. **Haibing He:** Conceptualization, Project administration, Supervision, Writing - review & editing.

Declaration of Competing Interest

The authors declare that they have no known competing financial interests or personal relationships that could have appeared to influence the work reported in this paper.

Acknowledgment

We were grateful for Amanda Pearce to correct the manuscript. This work was supported by the National Mega-project for Innovative Drugs [No.2019ZX09721001] and Program for Liaoning Innovative Talents in University [2012520007].

References

Bekaii-Saab, T.S., Villalona-Calero, M.A., 2005. Preclinical experience with docetaxel in gastrointestinal cancers. Semin. Oncol. 32, S3–S9.
Beloqui, A., Solinis, M.A., Gascon, A.R., del Pozo-Rodriguez, A., des Rieux, A., Preat, V., 2013. Mechanism of transport of saquinavir-loaded nanostructured lipid carriers across the intestinal barrier. J. Controlled Release 166, 115–123.
Beloqui, A., des Rieux, A., Preat, V., 2016a. Mechanisms of transport of polymeric and lipidic nanoparticles across the intestinal barrier. Adv. Drug Deliv. Rev. 106, 242–255.
Beloqui, A., Solinis, M.A., Rodriguez-Gascon, A., Almeida, A.J., Preat, V., 2016b. Nanostructured lipid carriers: promising drug delivery systems for future clinics. Nanomed. Nanotechnol. Biol. Med. 12, 143–161.
Beloqui, A., del Pozo-Rodríguez, A., Isla, A., Rodríguez-Gascón, A., Solinís, M.Á., 2017. Nanostructured lipid carriers as oral delivery systems for poorly soluble drugs. J. Drug Deliv. Sci. Technol. 42, 144–154.
Cheewatanakornkool, K., Niratisai, S., Manchun, S., Dass, C.R., Sriamornsak, P., 2017. Characterization and in vitro release studies of oral microbeads containing thiolated pectin–doxorubicin conjugates for colorectal cancer treatment. Asian J. Pharm. Sci. 12, 509–520.
Dimitroulis, I.A., 2014. Nintedanib: a novel therapeutic approach for idiopathic pulmonary fibrosis. Respiratory Care 59, 1450–1455.
Feng, S.S., Zhao, L.Y., Tang, J.T., 2011. Nanomedicine for oral chemotherapy. Nanomed. Nanotechnol. Biol. Med. 6, 407–410.
Fukihara, J., Kondoh, Y., 2016. Nintedanib (OFEV) in the treatment of idiopathic pulmonary fibrosis. Expert Rev. Respiratory Med. 10, 1247–1254.
Gurung, R.B., Purbe, B., Gyawali, P., Risal, P., 2013. The ratio of aspartate aminotransferase to alanine aminotransferase (AST/ALT): the correlation of value with underlying severity of alcoholic liver disease. Kathmandu Univ. Med. J. (KUMJ) 11, 233–236.
Harush-Frenkel, O., Rozentur, E., Benita, S., Altschuler, Y., 2008. Surface charge of nanoparticles determines their endocytic and transcytotic pathway in polarized MDCK cells. Biomacromolecules 9, 435–443.
Hu, F.-Q., Jiang, S.-P., Du, Y.-Z., Yuan, H., Ye, Y.-Q., Zeng, S., 2006. Preparation and characteristics of monostearin nanostructured lipid carriers. Int. J. Pharm. 314, 83–89.
Hubatsch, I., Ragnarsson, E.G., Artursson, P., 2007. Determination of drug permeability and prediction of drug absorption in Caco-2 monolayers. Nat. Protoc. 2, 2111–2119.
Iqbal, M.A., Md, S., Sahni, J.K., Baboota, S., Dang, S., Ali, J., 2012. Nanostructured lipid carriers system: recent advances in drug delivery. J. Drug Target. 20, 813–830.
Iqbal, M.A., Md, S., Mustafa, G., Kumar, M., Baboota, S., Sahni, J.K., Ali, J., 2014. Formulation, optimization and evaluation of nanostructured lipid carrier system of acyclovir for topical delivery. J. Bionanosci. 8, 235–247.
Kallus, S., Englinger, B., Senkiv, J., Laemmerer, A., Heffeter, P., Berger, W., Kowol, C.R., Keppler, B.K., 2018. Nanoformulations of anticancer FGFR inhibitors with improved therapeutic index. Nanomed. Nanotechnol. Biol. Med. 14, 2632–2643.
Kulkarni, S.A., Feng, S.S., 2013. Effects of particle size and surface modification on cellular uptake and biodistribution of polymeric nanoparticles for drug delivery. Pharm. Res. 30, 2512–2522.
Liu, Y., Zhang, J., Gao, Y., Zhu, J., 2011. Preparation and evaluation of glyceryl monooleate-coated hollow-bioadhesive microspheres for gastroretentive drug delivery. Int. J. Pharm. 413, 103–109.
Marzin, K., Kretschmar, G., Luedtke, D., Kraemer, S., Kuelzer, R., Schlenker-Herceg, R., Schmid, U., Schnell, D., Dallinger, C., 2018. Pharmacokinetics of nintedanib in subjects with hepatic impairment. J. Clin. Pharmacol. 58, 357–363.
Mishra, V., Bansal, K.K., Verma, A., Yadav, N., Thakur, S., Sudhakar, K., Rosenholm, J.M., 2018b. Solid lipid nanoparticles: emerging colloidal nano drug delivery systems. Pharmaceutics 10.
Mishra, D.K., Shandilya, R., Mishra, P.K., 2018a. Lipid based nanocarriers: a translational perspective. Nanomed. Nanotechnol. Biol. Med. 14, 2023–2050.
Mo, R., Jin, X., Li, N., Ju, C., Sun, M., Zhang, C., Ping, Q., 2011. The mechanism of enhancement on oral absorption of paclitaxel by N-octyl-O-sulfate chitosan micelles. Biomaterials 32, 4609–4620.
Muller, R.H., Radtke, M., Wissing, S.A., 2002. Solid lipid nanoparticles (SLN) and nanostructured lipid carriers (NLC) in cosmetic and dermatological preparations. Adv. Drug Deliv. Rev. 54, S131–S155.
Pardeike, J., Hommoss, A., Muller, R.H., 2009. Lipid nanoparticles (SLN, NLC) in cosmetic and pharmaceutical dermal products. Int. J. Pharm. 366, 170–184.
Pastor, M., Basas, J., Vairo, C., Gainza, G., Moreno-Sastre, M., Gomis, X., Fleischer, A., Palomino, E., Bachiller, D., Gutierrez, F.B., Aguirre, J.J., Esquisabel, A., Igartua, M., Gainza, E., Hernandez, R.M., Gavalda, J., Pedraz, J.L., 2019. Safety and effectiveness of sodium colistimethate-loaded nanostructured lipid carriers (SCM-NLC) against P. aeruginosa: in vitro and in vivo studies following pulmonary and intramuscular administration. Nanomed. Nanotechnol. Biol. Med. 18, 101–111.
Pradhan, M., Singh, D., Murthy, S.N., Singh, M.R., 2015. Design, characterization and skin permeating potential of Fluocinolone acetonide loaded nanostructured lipid carriers for topical treatment of psoriasis. Steroids 101, 56–63.
Reck, M., 2015. Nintedanib: examining the development and mechanism of action of a novel triple angiokinase inhibitor. Expert Rev. Anticancer Ther. 15, 579–594.
Reck, M., Kaiser, R., Mellemgaard, A., Douillard, J.-Y., Orlov, S., Krzakowski, M., von Pawel, J., Gottfried, M., Bondarenko, I., Liao, M., Gann, C.-N., Barrueco, J., Gaschler-Markefski, B., Novello, S., 2014. Docetaxel plus nintedanib versus docetaxel plus placebo in patients with previously treated non-small-cell lung cancer (LUME-Lung 1): a phase 3, double-blind, randomised controlled trial. Lancet Oncol. 15, 143–155.
Ren, T., Wang, Q., Xu, Y., Cong, L., Gou, J., Tao, X., Zhang, Y., He, H., Yin, T., Zhang, H., Zhang, Y., Tang, X., 2018. Enhanced oral absorption and anticancer efficacy of cabazitaxel by overcoming intestinal mucus and epithelium barriers using surface polyethylene oxide (PEO) decorated positively charged polymer-lipid hybrid nanoparticles. J. Controlled Release 269, 423–438.
Roth, G.J., Binder, R., Colbatzky, F., Dallinger, C., Schlenker-Herceg, R., Hilberg, F., Wollin, S.L., Kaiser, R., 2015. Nintedanib: from discovery to the clinic. J. Med. Chem. 58, 1053–1063.
Sahay, G., Alakhova, D.Y., Kabanov, A.V., 2010. Endocytosis of nanomedicines. J. Controlled Release 145, 182–195.
Shah, N.V., Seth, A.K., Balaraman, R., Aundhia, C.J., Maheshwari, R.A., Parmar, G.R., 2016. Nanostructured lipid carriers for oral bioavailability enhancement of raloxifene: Design and in vivo study. J. Adv. Res. 7, 423–434.
Vaidya, B., Shukla, S.K., Kolluru, S., Huen, M., Mulla, N., Mehra, N., Kanabar, D., Palakurthi, S., Ayehunie, S., Muth, A., Gupta, V., 2019. Nintedanib-cyclodextrin complex to improve bio-activity and intestinal permeability. Carbohydr. Polym. 204, 68–77.
Varadi, J., Harazin, A., Fenyvesi, F., Reti-Nagy, K., Gogolak, P., Vamosi, G., Bacskay, I., Feher, P., Ujhelyi, Z., Vasvari, G., Roka, E., Haines, D., Deli, M.A., Vecsernyes, M., 2017. Alpha-melanocyte stimulating hormone protects against cytokine-induced barrier damage in Caco-2 intestinal epithelial monolayers. PLoS One 12, e0170537.
Yanagiba, Y., Suzuki, T., Suda, M., Hojo, R., Gonzalez, F.J., Nakajima, T., Wang, R.S., 2016. Cytochrome P450 2E1 is responsible for the initiation of 1,2-dichloropropane-induced liver damage. Toxicol. Ind. Health 32, 1589–1597.
Yuan, H., Wang, L.L., Du, Y.Z., You, J., Hu, F.Q., Zeng, S., 2007. Preparation and characteristics of nanostructured lipid carriers for control-releasing progesterone by melt-emulsification. Colloids Surf. B, Biointerfaces 60, 174–179.
Zhang, K., Lv, S., Li, X., Feng, Y., Li, X., Liu, L., Li, S., Li, Y., 2013. Preparation, characterization, and in vivo pharmacokinetics of nanostructured lipid carriers loaded with oleanolic acid and gentiopicrin. Int. J. Nanomed. 8, 3227–3239.